Int. J. Electrochem. Sci., 14 **(2019)** 11081 – 11091, doi: 10.20964/2019.12.55

International Journal of
ELECTROCHEMICAL
SCIENCE
www.electrochemsci.org

Functionalization of Multiwalled Carbon Nanotubes using Cold Plasma Treatment and their Electrochemical Performances

L. L. Guo[1], Z.H. Luo[1,], Y.Z. Zhao[1], J. Guo[1], M. Zhu[1], K. Luo [1,*], A. Z. Huang[2]*

[1] Guangxi Key Laboratory of Universities for Clean Metallurgy Comprehensive Utilization of Nonferrous Metal Resource, Guilin University of Technology, Guilin, 541004, PR China
[2] Humanwell Healthcare (GROUP)CO., LTD, Wuhan, 430075, PR China
[*]E-mail: luozhihong615@glut.edu.cn, luokun@glut.edu.cn

Received: 7 August 2019 / *Accepted:* 17 September 2019 / *Published:* 29 October 2019

Functionalization of multiwalled carbon nanotubes (MWNTs) are proceeded with cold plasma generated in N_2 and air atmosphere. X-ray photoelectron spectroscope (XPS) shows that the nitrogen and/or oxygen elements are incorporated into MWNTs. The total nitrogen contents are approximately equal in N_2 and air atmospheres, while oxygen content is increased significantly in air atmosphere, the species and content of the functional groups depend on the applied gases. Transmission electron microscope (TEM) shows that the morphology of functionalized MWNTs is almost the same to pristine MWNTs, although functional groups and defects increase. The electrochemical experiments results demonstrate that introduction of functional groups enhance the pseudocapacitance, while the cyclic stability of the functionalized MWNTs is as well as the pristine MWNTs.

Keywords: Cold plasma, Multiwalled carbon nanotubes, Functionalization, Supercapacitor

1. INTRODUCTION

Carbon nanotubes (CNTs) have attracted tremendous attentions for their outstanding mechanical properties, conductivity, huge specific surface area and chemical stability, [1] which have been used in various fields, such as electronic device, batteries, supercapacitors, and et al. However, the inert surface properties of pristine CNTs limit their applications due to the weak interaction with other materials and poor wettability. Nowadays, functionalization such as heteroatom doping, surfactant or polymer modification is applied to improve the above mentioned properties. Surfactant (or polymer) and CNTs are combined by covalent bond without destroying intrinsic character of CNTs [2-3], however, the conductivity of modified CNTs is decreased due to the insulated surfactant and polymer, thus this kind of modified CNTs is not suitable for the circumstances which require high conductivity, such as the field of batteries, supercapacitors and other energy storage devices.

Heteroatom doping is widely applied to functionalize carbon nanotubes, even other carbon materials, such as, graphene, carbon nanofibers. The heteroatoms, for example, N, O, B, S and P can improve the conductivity and wettability. [4-7] Among which, N doping is widely used because nitrogen groups can significantly enhance the performance of supercapacitors and batteries, even nitrogen doped carbon materials can be used as metal-free electrocatalysts for oxygen reduction reactions. [8] Previous studies demonstrated that nitrogen doped carbon materials can be prepared with the following methods: (1) graphitizing nitrogen contained precursor via chemical vapor depositing, direct current magnetron sputtering andetc; [9-11] (2) carbonizing nitrogen-rich polymer or precursors; [12-13] (3) post treating the carbon materials in the nitrogenous atmosphere, such as N_2 and/or NH_3 and etc. [14-17]

By using the first methods, nitrogen exists in the internal and external wall of CNTs resulting in high nitrogen content and wall torsion. Suenaga and co-workers found that the nitrogen content was in the range from 13 at.% to 30 at.% by adjusting the ratio of N_2/Ar with direct current magnetron sputtering. [9] Liu and co-workers' reported that the morphology transformed from straight and smooth walls to cone-stacked shape or bamboo-like structure with increasing of nitrogen content by using a floating catalyst chemical vapor deposition method. [10] However, the device is complicated and expensive. Compared to the first methods, the preparation of N-CNTs with the second methods is facile to realize, but careful control of raw materials' morphology and carbonization condition are needed to form the tubular structure. With the application of the third methods, heat, plasma or N_2^+ ion beam, ball milling and etc are employed to prepare N-CNTs with the improved property while the original morphology and structure of CNTs is almost unchanged. During which, plasma or N_2^+ ion beam treatment is an environment-friendly, time-saving method to functionalize CNTs, however vacuum environmental is required, and the structure of CNTs is destroyed when the high energy beam is applied, [13] more milder methods are needed to explore.

It is reported that cold plasma treatment is used to functionalize materials in ambient temperature and pressure with low destruction. [18-20] In this paper, N_2 and/or air-generated cold plasma are adopted to functionalize MWNTs by using home-made plasma generator without high temperature and vacuum, the time required for nitrogen doping is short and no post treatment processes are needed. The content and species of nitrogen groups, as well as oxygen groups induced by N_2 and/or air are investigated comparatively, where the total nitrogen content is about 0.9 at.%, oxygen content increased about 2.4 at.% in air, the species of functional groups are varied with the applied gases. The electrochemical behavior and the effect of functional groups on the performance of functionalized MWNTs are studied in detail, by incorporation of functional groups, the specific capacitance is increased while the cyclic stability is maintained.

2. EXPERIMENTS

2.1 Materials

Raw multi-walled carbon nanotubes with 5-15 μm in length and 20-50 nm in diameter were purchased from Shenzhen Nanotech Porch Co., Ltd., China. N_2 with the purity of 99.9% and air pumped from atmosphere were used to generate plasma.

2.2 Cold plasma treatment of MWNTs

The home-made cold plasma device was used to functionalize MWNTs with corona discharge mode. A plasma generator was connected to a discharge chamber with two nickel electrodes wrapped on its outer wall. The cold plasma can be generated when the gas passed through the chamber and the voltage was applied between the two electrodes. In this paper, the gas was partly excited by using alternating current (AC) with a voltage amplitude value of 50 V and a power of 21 W. Before power on, the remained gas in the container was removed flowing gas for 30 min. The plasma flowed with the gas through a bush to blow from the bottom of container where pristine MWNTs were placed and to functionalize MWNTs. All the cold plasma treatment process lasted 30 min during which the process was paused to cool down the device in every 2 min. The samples treated by the N_2 and air-generated cold plasma were named as MWNT-N and MWNT-A, respectively.

2.3 Characterization

The element composition of the samples was measured on X-ray photoelectron spectroscopic instrument (XPS, ESCALAB250Xi, Thermo). Raman spectra were obtained on a Thermo Fisher DXR Raman spectrometer equipped with a 532 nm incident laser light source. The morphology images were obtained on Field emission transmitting electron microscopy (TEM, JEOL, JEM-2100F) in low vacuum mode. XRD spectra were recorded on X- ray diffractometer (XRD, X' Pert PRO).

2.4 Electrochemical measurements

All electrochemical measurements were performed in a three-electrode setup. Pt foil and saturated calomel electrode (SCE) was used as counter and reference electrode, respectively, and 6 mol L^{-1}KOH was used as electrolyte. The working electrode was prepared by mixing 20 μL of ethanol, 10 mg of as-prepared samples, 10 μL of 5% poly(tetrafluoroethylene) (PTFE) to obtain slurry which was pressed on the nickel foam substrates(1 cm ×1 cm) and dried at 60 °C for 5 h.

3. RESULTS AND DISCUSSION

N_2 and air generated cold plasma are used to modify the surface of multi-wall carbon nanotubes, respectively. As the illustration showed in Fig.1, air (mainly includes N_2 and O_2) or N_2 is ionized to form plasma during the discharge process. The cold plasma sprays through the airbrush and acted on MWNTs to create functional groups on the surface or subsurface of carbon. The illustration is showed in Fig.1. The flame image is Ar plasma because its blue flame is obvious to observe.

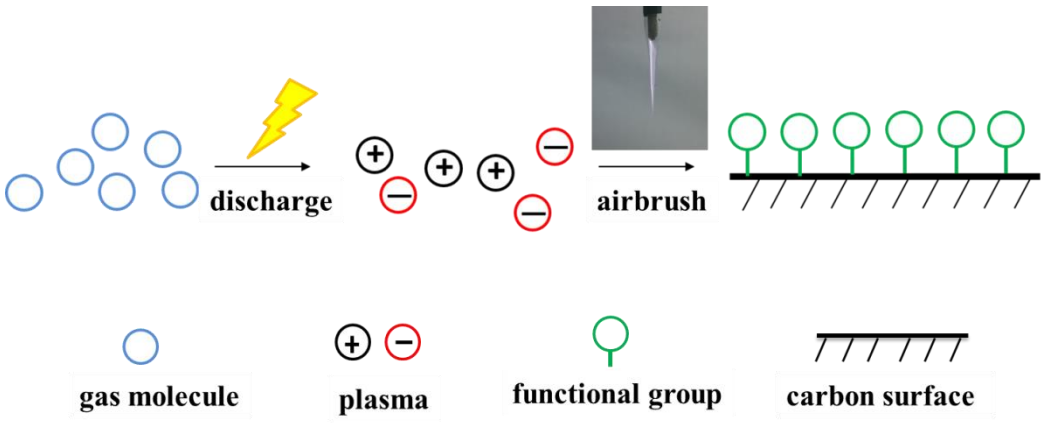

Figure 1. Illustration for functionalization of MWNTs by cold plasma treatment.

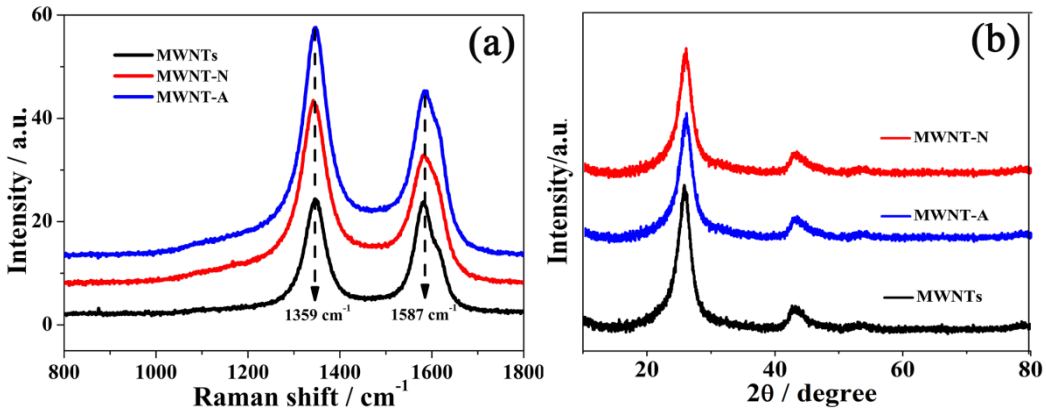

Figure 2. Raman (a) and XRD pattern (b) of MWNTs, MWNT-N and MWNT-A.

The structure of functionalized MWNTs is measured by Raman and XRD analysis. Fig. 2a shows the Raman spectra of MWNT-N, MWNT-A and the original MWNT, and peak at 1359 cm^{-1} correspond to the disordered (D) band, due to the breathing pattern of the A_{1g} symmetric κ point photon, which is related to the defects in graphitic structure. The peak located at 1587 cm^{-1} corresponds to the G band, attributed to the vibration in all sp^2 bonded carbon atoms due to the E_{2g} mode. [21] The high intensity of D band of MWNTs is due to the post acid-treatment for removing metal catalyst. The I_D/I_G ratio of MWNTs (about 1) increases to 1.35 and 1.34 after N_2 and air cold plasma treatments, respectively. The increased I_D/I_G ratio demonstrates the increased defects of MWNTs because of the formation of functional groups. The XRD pattern is used to characterize the structure of nitrogen doped MWNTs. Two characteristic peaks located at around 25.6° and 42° correspond to the (002) and (100) planes of hexagonal carbon. [22]

TEM images (Fig. 3) show the morphology of MWNTs, MWNT-N and MWNT-A, all the samples exhibit a smooth, long and tortuous morphology, which is similar to pristine MWNTs. No notch and distortion are observed, the open ends of the carbon nanotubes are the position where the metal catalysts are removed by acid treatment before delivery. The unbroken tubes of MWNT-N and MWNT-A implies that the cold plasma act on the surface and/or subsurface of MWNTs without

serious damaging the structure, which elucidate that cold plasma treatment is a low destructive method for functionalization.

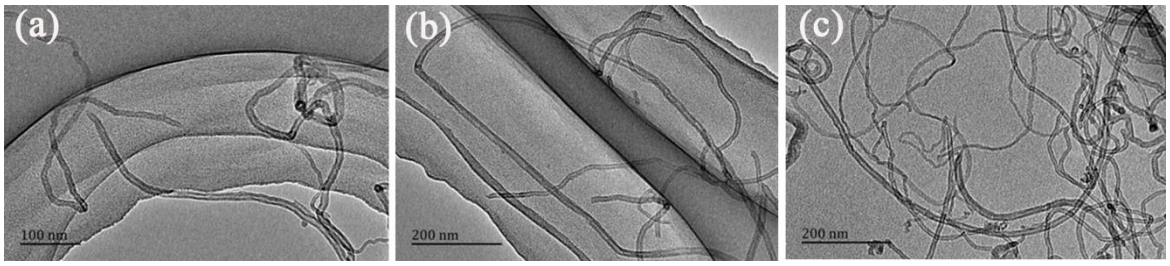

Figure 3. TEM images of MWNTs(a), MWNT-N(b) and MWNT-A(c)

The distribution of surface nitrogen, oxygen functionalities of MWNTs, MWNT-N and MWNT-A are measured by the deconvolution of corresponding N1s and O1s high-resolution XPS signals, which are illustrated in Fig.4, Table 1 and Table 2. As showed in Table 1, the N and O species of pristine MWNTs are probable from the impurity in synthesis and post acid-treatment process. Nitrogen element is incorporated into MWNTs by N_2 and air cold plasma treatment effectively, with the N atom percentage increasing from 0.39 at.% (MWNTs) to 0.9 at.% (MWNT-N) and 0.94 at.% (MWNT-A), respectively. Moreover, the oxygen content of MWNT-A is increased about 2.4 at.%, for MWNT-N, the oxygen content (1.02 at.%) is almost equal to MWNTs (1.03 at.%).

Table1. C, O, N element content of MWNTs, MWNT-N, MWNT-A.

Species	At. %		
	MWNTs	MWNT-N	MWNT-A
C1s	96.83	96.07	90.19
O1s	1.03	1.02	3.47
N1s	0.39	0.9	0.94

The chemical states of nitrogen atoms with binding energies about 398.7 eV, 399.5 eV, 401.4 eV, 405.0 eV and 406.1 eV are identified as pyridine (N-6), pyrrole (N-5), quaternary nitrogen (N-Q) and pyridine-N-Oxide (N^+-O^-) and -NO_2, respectively. [23] As Fig. 4a-c and Table 2 shows, nitrogen species of pristine MWNTs are mainly N-6, N-5, N-Q and a small amount of N^+-O^-. As for MWNT-N, the content of N-6, N-5, N-Q and N^+-O^- increase, the oxygen in N^+-O^-group possibly originates from the impurity of N_2 gas. As for MWNT-A, the content of N-6 increases compared to pristine MWNTs, while N-5 disappears possibly because N-5 is unstable in the oxidized atmosphere, [24] and oxygen-contained nitrogen species, such as N^+-O^- (0.41 at.%) and -NO_2 (0.31 at.%) increase significantly.

As for oxygen groups, the peaks at about 532.9 eV, 532.0 eV, 531.2 eV and 530.5 eV are attributed to C-OH, C=O, pyridine-N-oxide (N^+-O^-), and HO-C=O (-NO_2), respectively. [25] It is worth noting that the -COOH group disappears in MWNT-N, the content of pyridine-N-oxide increases, the C-OH and C=O is almost identical to pristine MWNTs, which results in the oxygen content unchanged. While for MWNT-A, the C-OH groups vanished, -COOH and C=O groups

increase significantly. The content of -NO_2 and -COOH groups is calculated to be 0.84 at.% and 0.62 at.% (the content of -COOH is calculated by subtracting doubled value of -NO_2 (at 406.1 eV) from the total content obtained from peak at 530.5 eV). These results demonstrate that the functional groups introduced into MWNTs depend on the applied gases.

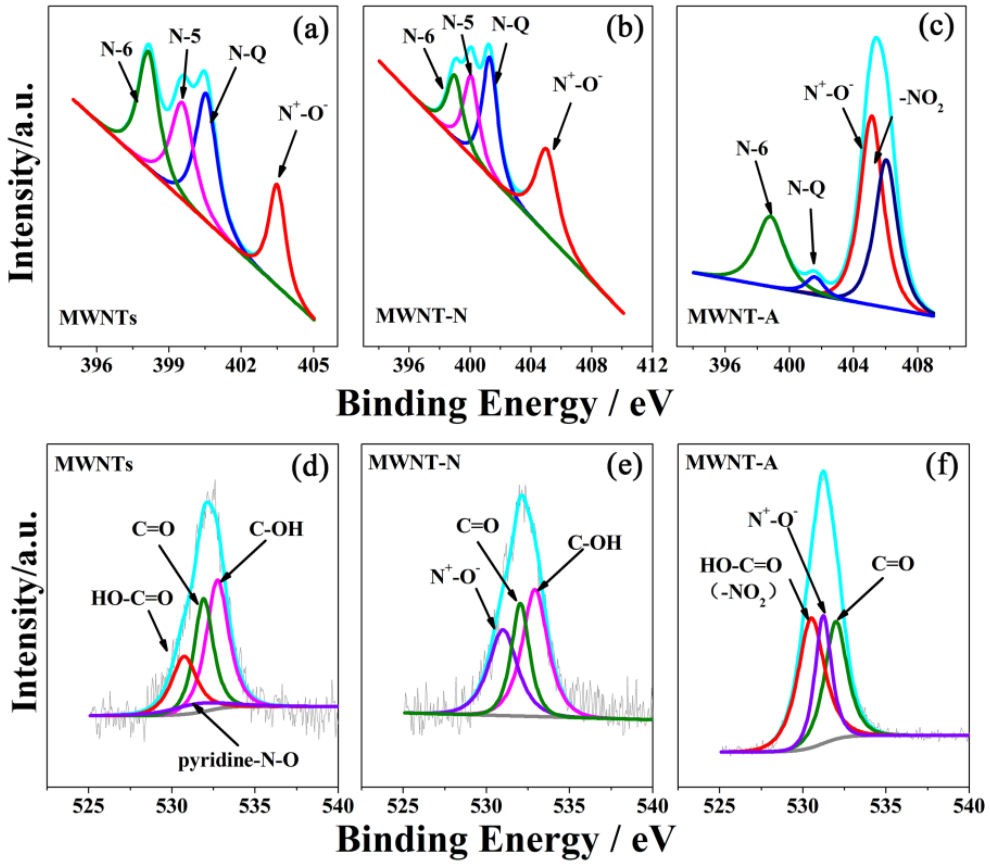

Figure 4. XPS spectra of N1s (a, b, c) and O1s (d, e, f) spectra of MWNTs (a, d), MWNT-N(b, e) and MWNT-A(c, f).

Table 2. Nitrogen and oxygen species content of MWNTs, MWNT-N, MWNT-A

Species		At. %		
		MWNTs	MWNT-N	MWNT-A
N	N-6	0.1	0.15	0.19
	N-5	0.09	0.19	N/A
	N-Q	0.12	0.28	0.03
	N^+-O^-	0.07	0.29	0.41
	-NO_2	N/A	N/A	0.31
O	HO-C=O	0.25	N/A	0.84
	N^+-O^-	0.06	0.33	0.89
	C=O	0.31	0.27	2.67
	C-OH	0.41	0.43	N/A
	-NO_2	N/A	N/A	0.62

N/A means that the species are not detected

The effect of functional groups on the electrochemical properties is estimated by using cyclic voltammetry (CV), galvanostatic charge-discharge and electrochemical impedance spectroscopy (EIS). Fig. 5 shows the CV curves of carbon nanotubes in 6 M KOH. It shows that all samples display a couple of redox peaks although which are not obvious in pristine carbon nanotube. The redox peaks are mainly originated from faradic current caused by the existence of active nitrogen and/or oxygen groups, because the redox peaks still preserve in the Ar saturated electrolyte (which is not showed here) and no redox peaks are observed on bare nickel foam (inset of Fig.5). The MWNT-N exhibits the highest reduction current density, followed by MWNT-A and MWNTs.

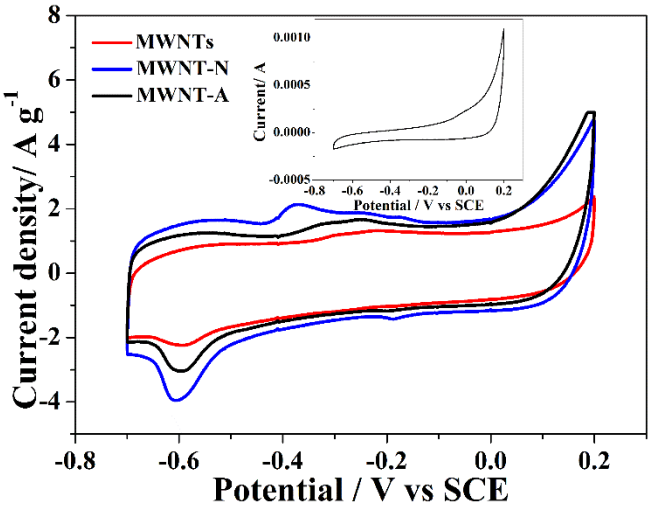

Figure 5. CV curves of MWNTs, MWNT-N and MWNT-A at 25 mV s^{-1}, inset: CV curve of bare nickel foam.

The galvanostatic charge-discharge curves are showed in Fig.6a and 6b. Due to the existence of faradic current, the charge-discharge curves deviated from linearity, especially for MWNT-N and MWNT-A at low current density. At high current density, the deviation is alleviated demonstrating the main contribution of EDLC at rapid charge-discharge process.

The specific capacitance is calculated from charge-discharge curves from the equation:

$$C = \frac{I\Delta t}{mV} \qquad (1)$$

Where C is the specific capacitance (F g^{-1}), I is the charge-discharge current (A), Δt is the discharge time (s), m is the mass of electrode materials (g), V is the potential window (ΔV).

The specific capacitances of MWNTs, MWNT-A and MWNT-N are showed in Fig.6c. The highest specific capacitance of 87 Fg^{-1} is obtained from MWNT-N. At the current density of 0.2 Ag^{-1}, 0.5 Ag^{-1}, 1.0 Ag^{-1}, 2.0 Ag^{-1}, the specific capacitance of MWNT-N is 87 Fg^{-1}, 59 Fg^{-1}, 44 Fg^{-1}, 40 Fg^{-1}, respectively, which increases 40% more than that of MWNTs, especially at the current density of 0.2 Ag^{-1}, the capacitance increases by 52.6% demonstrating significant contribution of pseudocapacitance. MWNT-N exhibits the highest capacitance at each current density, followed by MWNT-A and MWNTs. Fig.6d shows the cyclic stability of MWNTs, MWNT-N and MWNT-A, in which the

capacitance retention decrease fast at the first 30 cycles, possibly due to the fast decay of the pseudocapacitance, after then these three samples can keep stable at least 4000 cycles with the capacitance retention about 79.3%, 82.5% and 79.5% for MWNTs, MWNT-N and MWNT-A, respectively. Here, we compared the specific capacitance values of different carbon-based materials. [26-29,32] The specific capacity of MWNT-N in this paper is higher than other carbon-based materials in the literature, as shown in Table 3.

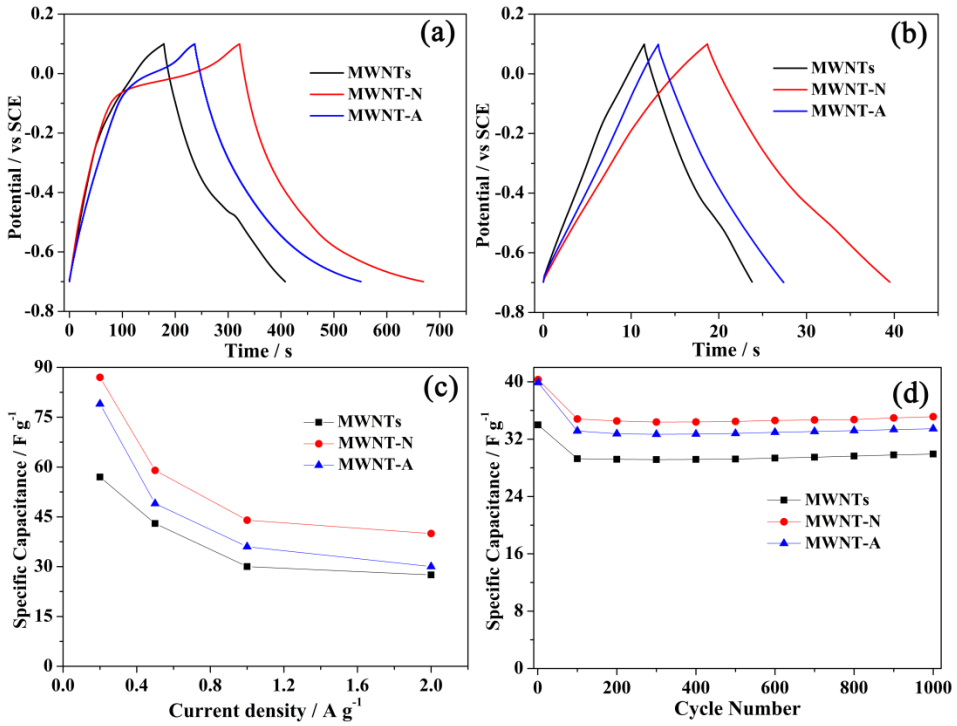

Figure 6. Charge-discharge curves of MWNTs, MWNT-N and MWNT-A at the current density of 0.2 Ag^{-1}(a) and 2 Ag^{-1}(b). Specific capacitance (c) and cycling stability (d) of MWNTs, MWNT-N and MWNT-A.

Table 3. Specific capacitance comparison between plasma treated MWNTs and other materials

Types of materials	Specific capacitance (F g^{-1})	Reference
MWNT-N	87	This work
RFN700	18.67	Ref. 32
P-MWNT	14.36	Ref. 26
N-o-FMWCNT	62.7	Ref. 26
N-i-FMWCNT	37	Ref. 26
SWCNT	35	Ref. 27
MnO_2/CNT	44	Ref. 28
Au-MnO_2/CNT	68	Ref. 28
IrO_2NT/CNT	69	Ref. 29

According to the previous reports, N-5, N-6, C=O and C-OH contribute to the pseudocapacitance, [30] N-6 and N-Q improved the conductivity of carbon materials. [31] The total content of N-5, N-6, N-Q, C=O and C-OH groups of MWNT-N are higher than those of MWNTs and MWNT-A, leading to higher pseudocapacitance. As for MWNT-A, the high content of C=O and N-6 improve their pseudocapacitance, however, compared to MWNT-N, the sum of N-6 and N-Q is lower, and the total content of N^+-O^-, -NO_2 and -COOH is higher, which could hinder the enhancement of supercapacitor performance.

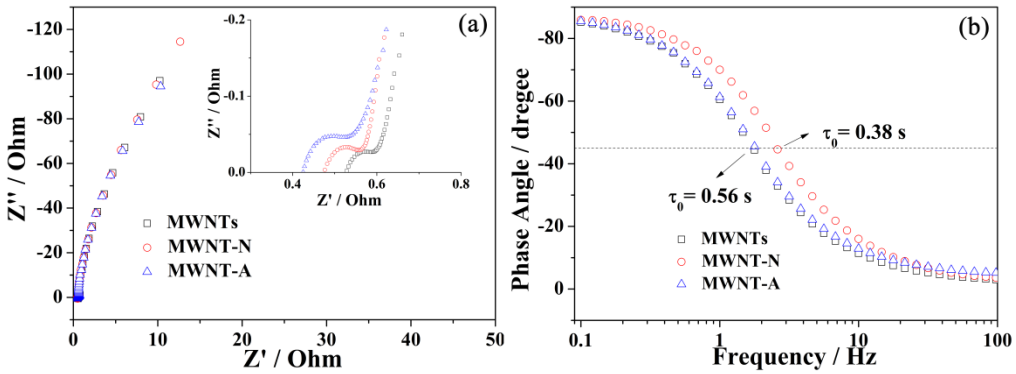

Figure 7. Nyquist plots (Figure 7a, inset: Nyquist plots at high frequency) and Bode plots (Figure 7b) of MWNTs, MWNT-N and MWNT-A.

To further understand their capacitive behaviors, the Nyquist plots of MWNTs, MWNT-N and MWNT-A are showed in Fig.7a, where the frequency ranges from 100 kHz to 0.01 Hz. All the Nyquist plots contain two parts: a semicircle and a straight line. As showed in the inset of Fig.7a, the intercept of horizontal axis which represents the equivalent series resistance (ESR) is reduced, possibly due to improvement of the wettability and conductivity caused by nitrogen and oxygen groups. [32]The small uncompleted semi-circle of each plot at high frequency demonstrates low charge transfer resistance, which indicates the high conductivity of nitrogen doped carbon nanotubes. The characteristic frequency f_0 at the phase angle of -45° is 2.61 Hz for MWNT-N and 1.78 Hz for MWNTs and MWNT-A, corresponding to the time constant τ_0 ($\tau_0=1/f_0$) of 0.38 s and 0.56 s, respectively, the shorter time constant of MWNT-N indicates the faster charge-discharge rate compared to MWNT and MWNT-A. [33]

Based on the results, we consider that cold plasma is a green and facile method to modify carbon materials, where only functionalities and no other agents who influence the purity of carbon materials are introduced. Although the electrochemical performance is improved because of functionalization, the nitrogen groups content and specific capacitance of functionalized MWNTs are needed to enhance in future work.

4. CONCLUSION

Nitrogen and oxygen groups are introduced to MWNTs with cold plasma treatment successfully. The content of introduced nitrogen is almost the same by using N_2 and air, however, the

species of functional groups are different, the oxygen is introduced with considerable high content by using air. The morphology of pristine carbon nanotubes is preserved, while the disorder and defects are increased. The specific capacitance is increased for MWNT-N and MWNT-A, and the cyclic stability is maintained. We consider that the cold plasma treatment is a mild and effective method to functionalize the carbon materials without destroying the structure seriously, which also can be used for other carbon materials, such as graphene, carbon nanofibers and etc.

ACKNOWLEDGEMENTS
This work was supported by Guangxi Natural Science Foundation and National Natural Science Foundation of China (No. 2016GXNSFAA380107, 2018GXNSFAA281184 and 51874051) and the funding from Key Lab of New Processing Technology for Nonferrous Metals & Materials Ministry of Education and Featured Materials and Collaborative Innovation Center for Exploration of Hidden Nonferrous Metal Deposits and Development of New Materials in Guangxi.

References

1. Z. B. Yang, J Ren, Z. T. Zhang, X. L. Chen, G. Z. Guan, L. B. Qiu, Y Zhang, H. S. Peng, *Chem. Rev.*, 115 (2015) 5159.
2. T. Morishita , M. Matsushita, Y. Katagiri, K. Fukumori, *Carbon*, 48 (2010) 2308.
3. L. Mao, K. Zhang, H. S. O. Chan, J. S. Wu, *J. Mater. Chem.*, 22 (2012) 80.
4. J. Liang, Y. Jiao, M. Jaroniec, S. Z. Qiao, *Angew. Chem.*, 124 (2012) 11664.
5. Z. B Tian, C. Liu, Q. Y Li, J.Y Hou, Y. Li, S.Y Ai, *Appl. Catal. A : General.*, 506 (2015) 134.
6. T. X. Shang, X. X. Cai, X. J. Jin, *RSC Adv*., 5 (2015) 16433.
7. X. D Ren, J. Z Zhu, F. M Du, J. J Liu, W. Q Zhang, *J. Phys. Chem. C.*, 118 (2014) 22412.
8. Q. H. Guo, D. Zhao, S. W. Liu, S. L. Chen, M. Hanif, H. Q. Hou, *Electrochim. Acta*, 138 (2014) 318.
9. K. Suenaga, M.P. Johansson, N. Hellgren, E. Broitman, L.R. Wallenberg, C Colliex, J.E. Sundgren, L. Hultman, *Chem. Phys. Lett.*, 300 (1999) 695.
10. H. Liu, Y. Zhang, R.Y. Li, *Carbon*, 48 (2010) 1498.
11. V. Eckert, A. Leonhardt, S. Hampel, B. Büchner, *Diamond Relat Mater*., 86 (2018) 8.
12. N. Gavrilov, I. A. Pašti, M. Vujkovic, *Carbon*, 50 (2012) 3915.
13. Q. Liu, Z. H. Pu, C. Tang, A. M. Asiri, A. H. Qusti, A. O. Al-Youbi, X. P. Sun, *Electrochem. Commun*, 36 (2013) 57.
14. F. Xu, M. Minniti, P. Barone, A. Sindona, A. Bonanno, A. Oliva, *Carbon*, 46 (2008) 1489.
15. P. M. Dong, X. D. Cheng, Z. Jin, Z. .F. Huang, X. X. Nie, X. Y. Wang, X. W. Zhang, *J Photochem Photobiol A: Chemistry*., 382 (2019) 111971.
16. Q. Q. Chen, A Ozkan, B. Chattopadhyay, K. Baert, C. Poleunis, A. Tromont, R. Snyders, A. Delcorte, H. Terryn, M-P D-Ogletree, Y. H. Geerts, F. Reniers, *Langmuir*, 35 (2019) 7161.
17. J. Y. Yook, J. Jun, S. Kwak, *Appl. Surf. Sci.*, 256 (2010) 6941.
18. F.Poncin-Epaillard, J.C.Brosse, T.Falher, *Macromolecules*, 30 (1997) 4415.
19. V. K. Abdelkader., S. Scelfo. C. García-Gallarín, M. L. Godino-Salido, M. Domingo-García, F. Javier López-Garzón, M. Pérez-Mendoza, *J. Phys. Chem. C.*, 117 (2013), 16677.
20. O. Chirila, M. Totolin, G. Cazacu, M. Dobromir, C. Vasile, *Ind. Eng. Chem. Res.*, 52 (2013) 13264.
21. Z. H. Luo, L. H. Zhu, Y. F. Huang, H. Q. Tang, *Synth. Met*., 175 (2013) 88.
22. S. B. Wang, C.L. Xiao, Y. L. Xing, H. Z. Xu, S. C. Zhang, *J .Mater. Chem. A.*, 3 (2015) 6742.
23. M. Vujković, N.Gavrilov, I. A. Pašti, *Carbon*, 64 (2008) 472.

24. H. Sjöström, S. Stafström, M. Boman, J.-E. Sundgrn, *Phys. Rev. Lett.*, 75 (1995) 1336.
25. H. L. Wang, Q. L. Hao, X. J. Yang, L. D. Lu, X. Wang, *ACS Appl. Mater. Interfaces*, 2 (2010) 821.
26. R. Qin, Q. L Qian, Y. Liu, A. P. Ou, Y. L. Li, X. Liu, X. Y. Liu, X. Wang, *J. Phys. Chem, C*., 123 (2019) 16439.
27. Z. Q. Niu, W. Y. Zhou, J. Chen, G. X. Feng, H. Li, W. J. Ma, J. Z. Li, H. B. Dong, Y. Ren, D. Zhao, S. S. Xie, *Energy Environ. Sci*., (4) 2011 1440.
28. A. L. M. Reddy, M. M. Shaijumon, S. R. Gowda, P. M. Ajayan, *J. Phys. Chem. C., 114 (*2010) 658.
29. Y. M. Chen, J. H. Cai1, Y. S. Huang, K. Y. Lee, D. S. Tsai, *Nanotechnology*, 22 (2011) 115706.
30. H. Y. Liu, H. H. Song, X. H. Chen, S. Zhang, J. S. Zhou, Z. K. Ma, *J. Power Sources*, 28 (2015) 5303.
31. W. Fan, Y. E. Miao, L. S. Zhang, Y. P. Huang, T. X. Liu, *RSC Adv.*, 5 (2015) 31064.
32. S. L. Candelaria, B. B. Garcia, D.W. Liu, G. Z, Cao, *J. Mater. Chem.*, 22 (2012) 9884.
33. J. Zhao, H. W. Lai, Z. Y. Lyu, Y. F. Jiang, K. Xie, X. Z. Wang, Q. Wu, L. J. Yang, Z. Jin, Y. W. Ma, J. Liu, Z. Hu, *Adv. Mater*., 27 (2015) 3541.